Electric propulsion system scaling for asteroid capture-and-return missions

Justin M. Little* and Edgar Y. Choueiri†

Electric Propulsion and Plasma Dynamics Laboratory, Princeton University, Princeton, NJ, 08544

The requirements for an electric propulsion system needed to maximize the return mass of asteroid capture-and-return (ACR) missions are investigated in detail. An analytical model is presented for the mission time and mass balance of an ACR mission based on the propellant requirements of each mission phase. Edelbaum's approximation is used for the Earth-escape phase. The asteroid rendezvous and return phases of the mission are modeled as a low-thrust optimal control problem with a lunar assist. The numerical solution to this problem is used to derive scaling laws for the propellant requirements based on the maneuver time, asteroid orbit, and propulsion system parameters. Constraining the rendezvous and return phases by the synodic period of the target asteroid, a semi-empirical equation is obtained for the optimum specific impulse and power supply. It was found analytically that the optimum power supply is one such that the mass of the propulsion system and power supply are approximately equal to the total mass of propellant used during the entire mission. Finally, it is shown that ACR missions, in general, are optimized using propulsion systems capable of processing 100 kW – 1 MW of power with specific impulses in the range 5,000 – 10,000 s, and have the potential to return asteroids on the order of $10^3 - 10^4$ tons.

Nomenclature

a_f = semi-major axis
C_P = power coefficient
e_f = eccentricity
f_j = acceleration of j^{th} maneuver
I_{sp} = specific impulse
J = cost function
u_e = effective exhaust velocity
r_a = orbit apsis
r_p = orbit periapsis
r_{leo} = low-Earth orbit radius
r_m = Moon orbit radius
t_f = final maneuver time
t_j = time of j^{th} maneuver
$t_{\min}$ = minimum possible maneuver time
t_{syn} = synodic period
α = propulsion and power system specific power
δ = spacecraft dry mass fraction
Δv_ζ = minimum possible delta-v
η = propulsion system efficiency
γ = angle of lunar assist delta-v
μ = ratio of returned asteroid mass to low-Earth orbit insertion mass
μ_e = Earth's gravitational parameter

*Graduate Student, Research Assistant
†Chief Scientist, EPPDyL, Professor, Applied Physics Group, AIAA Fellow

ν = normalized lunar assist delta-v
ρ = propulsion and power system mass fraction
τ = parameter governing non-optimal delta-v behavior
ξ = time-free minimum fuel trajectory scaling parameter
ζ_j = propellant mass fraction of j^{th} maneuver

I. Introduction

In just over a century since Konstantin Tsiolkovsky predicted that the advent of the rocket will ultimately enable human exploration of asteroids,[1] mankind has guided robotic spacecraft on scientific missions to eleven neighboring planetoids.[2–4] These missions have characterized asteroid structure and composition using advanced imaging and spectroscopic diagnostics, and have even returned surface samples to terrestrial research laboratories for detailed analysis, thus contributing to the understanding of solar system formation.

Recently, the Keck Institute for Space Sciences (KISS) published a study that investigated the feasibility of a robotic mission to capture and return an entire near-Earth asteroid (NEA) into a stable cis-lunar orbit to serve as a destination for future manned missions.[5] According to their report, a project of this magnitude promises to improve NEA detection techniques, advance high power electric propulsion technology, further understanding of asteroid composition and formation, and provide a testing platform for the development of asteroid resource extraction technology to support *in situ* resource utilization. These advances may ultimately provide a defense mechanism against potential asteroid impacts[6,7] and encourage a new space economy centered around asteroid resources.[8–11]

The feasibility of placing an asteroid into orbit around Earth was analyzed as early as Hills in 1992,[6] who concluded that decommissioned ICMs equipped with nuclear warheads could be used to force asteroids up to 170,000 tons into orbit around Earth for use as a planetary defense shield from potential impactors. Chemical rockets have been shown to be suitable for NEA rendezvous,[12] sample return missions,[13] and return missions of entire asteroids on the order of 100 tons to a stable Sun-Earth L2 orbit.[14] The required delta-v of the impulsive capture maneuver to an Earth orbit[10] compared to the relatively low specific impulse of chemical rockets renders them impractical for returning sizable (> 100 tons) asteroids to Earth orbit due to the excessive propellant requirement.

Multiple case studies have been performed for human exploration of NEAs[15,16] and asteroid capture-and-return (ACR) missions[5,17] using near-term, high-power electric propulsion technology. As a precursor to the KISS study,[5] it was found that a 10 ton NEA could be returned to the International Space Station (ISS) using a 40 kW solar electric propulsion system operating four 3,000 s specific impulse Hall thrusters.[17] In comparison, the KISS study determined that the same propulsion system may be capable of capturing and returning an 1,800 ton asteroid to cis-lunar space within a ten year mission span.[5] Both of these studies rely on lunar assists, which are shown to drastically reduce the propulsion system requirements and aid the insertion of the NEA and spacecraft into their final orbit.[18]

Literature in support of the technical capabilities of electric thrusters for ACR missions has only begun to emerge. Landau *et al.*[18] estimated the retrievable NEA mass as a function of the return trip time and asteroid orbit for the specific propulsion system chosen by the KISS study. Furthermore, they present six different cases that show the effect of changing the specific impulse and initial spacecraft mass (based on the launch vehicle size) on the maximum return mass for 40 kW of available power. Assuming constant acceleration and using a simplified dynamical model without lunar assist, Hasnain *et al.*[19] characterized the acceleration requirement to return an NEA to Earth orbit within a constrained mission time.

Missing from the literature is a general analysis of the relationship between the propulsion system and asteroid orbit and mass for ACR missions that utilize lunar assists. To help fill this gap, we propose to answer the following questions: *What are the electric propulsion system parameters that maximize the return mass of a given asteroid?* Furthermore, *how does the optimal electric propulsion system scale with the asteroid orbit and mass?* Notably, we will address the issue of the optimum specific impulse and power supply,[20,21] which becomes quite compelling for ACR missions based on two facts: (1) NEAs have been, and continue to be, found in a variety of different orbits,[22–24] and (2) the target becomes the payload.

II. ACR Mission Performance Model

We begin with a simplified theoretical model for an ACR mission. Following the analysis of the KISS study,[5] we separate the mission into three phases: (1) low-Earth orbit (LEO) to lunar gravity assist, (2) lunar gravity assist to asteroid orbit, and (3) asteroid orbit to lunar gravity assist.

The final mission time, t_m, may be expressed as

$$t_m = \sum_{j=1}^{3} t_j(\mu) + t_c, \tag{1}$$

where t_j is the transfer time of the j^{th} phase, and t_c is the time required to de-spin and capture the asteroid.

We extend the conventional, multi-stage, spacecraft mass conservation equation[25] to account for the addition of an added quantity of mass between the second and third mission phases. Defining the mass amplification ratio, μ, as the ratio of the asteroid mass to the total mass launched into LEO, the mass conservation equation takes the deceptively simple form

$$\mu = \frac{1}{\zeta_3}\left[\prod_{j=1}^{3}(1-\zeta_j)(1-\zeta_c) - \delta - \rho(t_m,\mu)\right]. \tag{2}$$

Here, ζ_j is the propellant mass fraction of the j^{th} mission phase, ζ_c is the propellant mass fraction required for capture operations, δ is the dry mass fraction of the spacecraft minus the power supply mass fraction, and ρ is the power supply mass fraction. Throughout the rest of our analysis we will ignore t_c and ζ_c because they are typically small compared to t_j and ζ_j, respectively.[5]

The functional dependences shown in Eqs. (1) and (2) emphasize the relationship between the asteroid mass, available power, and final mission time at a fixed specific impulse. For example, a more massive asteroid requires a larger power supply to move within a given time constraint than a less massive asteroid. Alternatively, for a fixed asteroid mass, the minimum transfer time decreases as the available power increases.[19] We also note that Eq. (2) stresses the previously observed sensitivity of the mass amplification ratio to the propellant mass fraction of the return phase, ζ_3.[18]

III. Trajectory Scaling

We develop in this section expressions for the propellant mass fraction as a function of the transfer time, propulsion system constraints, and asteroid orbit and mass. Using the patched conic approximation, we treat the Earth departure phase (1) in a geocentric reference frame and the asteroid rendezvous (2) and return (3) phases in a heliocentric reference frame. The lunar assist will be modeled as as part of the initial/final conditions of the later two phases.

Throughout our analysis we will model the problem as a central body (either the Earth or sun), and a point mass (either the lone spacecraft or the spacecraft with the captured asteroid). We neglect any outside gravitational perturbations and ignore time-dependent corrections to the available power, such as shadowing and degradation of solar panels. Furthermore, we restrict our analysis to the ecliptic plane, and assume that the asteroid has a negligible inclination ($i \approx 0$) with respect to the ecliptic.

A. Earth Departure

We base our analysis of the low-thrust transfer between LEO and the lunar gravity assist on a simplified model based on Edelbaum's approximation,[26] which assumes that in every revolution about the central body, the trajectory of the point mass remains nearly circular and the acceleration vector constant. Further assuming that the acceleration is directed along the motion of the point mass with magnitude f_1, the transfer time may be written as[25]

$$t_1 = \frac{\sqrt{\mu_e}}{f_1}\left(r_{\text{leo}}^{-1/2} - r_m^{-1/2}\right). \tag{3}$$

Here, μ_e is Earth's gravitational parameter, and r_{leo} and r_m are the orbital radii of LEO and the moon, respectively. The propellant mass fraction is then given by

$$\zeta_1 \approx \frac{f_1 t_1}{g_0 I_{\text{sp}}} = \frac{\sqrt{\mu_e}}{g_0 I_{\text{sp}}}\left(r_{\text{leo}}^{-1/2} - r_m^{-1/2}\right), \tag{4}$$

with g_0 the gravitational acceleration at Earth's surface and I_{sp} the specific impulse of the propulsion system. We have made the additional assumptions that $\zeta \ll 1$ and the I_{sp} is constant throughout the maneuver. These assumptions will be utilized throughout the remainder of the paper. We note that Eqs. (3) and (4) yield values consistent with those reported in the KISS study for this phase of the mission.[5]

B. Asteroid Rendezvous and Return

We seek a generalized scaling law for the time-bounded minimum-fuel (TBMF) propellant mass fraction for a transfer either to or from an arbitrary asteroid orbit. The solution will depend on the performance parameters of the propulsion system, asteroid mass, asteroid orbit, and desired transfer time.

As with many general low-thrust optimization studies,[27–29] our analysis is simplified by ignoring the phase difference between the departure orbit and the destination. The implications of this simplification are that the solution (1) is invariant with respect to the argument of periapsis of the target orbit, (2) represents the trajectory associated with the optimal departure date,[30] and (3) is time-invariant,[31] and may be used for either the rendezvous or return phases of the mission. Therefore, the scaling laws derived in this section should be viewed as an optimistic estimate for the propellant requirements of a given transfer.

1. Propellent Mass Fraction Semi-Empirical Model

The propellant mass fraction may be approximated as $\zeta \approx \Delta v / u_e$, where $u_e \equiv g_0 I_{\text{sp}}$ is the effective exhaust velocity of the propulsion system, and Δv is a metric for the energy imparted by the propulsion system on the spacecraft over the duration of a maneuver. We note the well-known fact that Δv is generally not equal to the change in orbital velocities for low-thrust transfers.

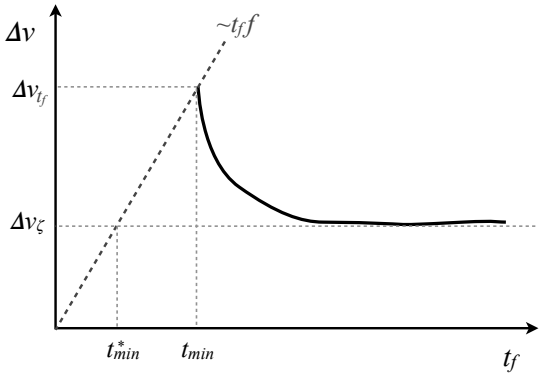

Figure 1. Qualitative scaling of the optimal Δv as a function of transfer time, t_f. The minimum-time minimum-fuel transfer time and delta-v are labeled as $t_{\min}$ and Δv_{t_f}, respectively. The time-free minimum-fuel delta-v is labelled as Δv_ζ. The dashed line corresponds to the theoretical delta-v that can be obtained in a given time following a "full-throttle" control law. $t^*_{\min}$ is the time corresponding to the intersection of Δv_ζ and the "full-throttle" line.

The qualitative dependence of the TBMF Δv as a function of the transfer time,[27,32] t_f, of a specific maneuver is depicted in Fig. 1. As the transfer time is increased, the spacecraft is able to apply thrust in the most energy-efficient manner, and Δv approaches an asymptote limited by the time-free minimum fuel (TFMF) problem, Δv_ζ. As the transfer time decreases, thrust must be applied at non-optimal times in order to complete the maneuver within the time constraint. This non-optimality leads to an increase in Δv, which ultimately approaches the minimum-time minimum-fuel (MTMF) value, Δv_{t_f}.

We now address the task of deriving an equation that is able to capture the salient characteristics of Fig. 1 in terms of variables that scale with the mission parameters. Based on the results of the following sections, we adopt the mathematical model for Δv as a function of t_f:

$$\Delta v = \left(e^{-ct_f^2} + \Delta v_\zeta\right) H^{-1}\left(t_f - t_{\min}\right). \tag{5}$$

Here, c is a constant that determines the shape of the non-optimal region of the curve and the value of $t_{\min}$. We include the Heaviside step function, $H\left(t - t_{\min}\right)$, in the denominator to ensure that $\Delta v \to \infty \; \forall \; t_f < t_{\min}$.

As we will confirm in Sec. 5, it is reasonable to assume that Δv_{t_f} will fall somewhere on the "full-throttle"-line described by $\Delta v = t_f f$, where f is the maximum acceleration provided by the propulsion system at the beginning of the transfer. Denoting the time at which Δv_ζ intersects the "full-throttle"-line as $t^*_{\min}$ (see Fig. 1), we further assume that $t_{\min} \approx \tau t^*_{\min}$, where τ is a factor that is larger than unity. Using these assumptions to eliminate c from Eq. (5) yields

$$\Delta v = \left\{[(\tau-1)\Delta v_\zeta]^{\left(\frac{t_f f}{\tau \Delta v_\zeta}\right)^2} + \Delta v_\zeta\right\} H^{-1}\left(t_f - t_{\min}\right). \tag{6}$$

Eq. (6) may be used to estimate the Δv required to perform a specified maneuver with acceleration, f, within the maneuver time, t_f. The optimal region of the curve asymptotes to Δv_ζ, while the shape of the non-optimal region is governed by the parameter τ. We will now show that numerical solutions to the TFMF and MTMF optimal control problems may be used to derive simple semi-empirical scaling relations for Δv_ζ and τ, respectively, as a function of the mission parameters.

2. Low-Thrust Trajectory Optimization

We treat the asteroid rendezvous and return phases of the mission within the context of the L^1-optimal control problem as described by Ross *et al.*[33,34]

The state and control vectors of the problem are given by

$$\mathbf{x}^T := [r, \theta, v_r, v_t] \qquad \mathbf{u}^T := [f, \beta], \tag{7}$$

subject to the constraint,

$$[0, -\pi] \leq \mathbf{u}^T \leq [f_\mathbf{j}, \pi]. \tag{8}$$

Here, f_j is the maximum acceleration, which depends on the maximum thrust and spacecraft mass for the rendezvous phase and spacecraft and asteroid masses for the return phase. The direction of the acceleration vector with respect to the polar coordinates is determined by β [as shown in Eq. (9)].

The trajectory optimization problem may be formulated as:[33]

$$O\left(a_f, e_f, f_j\right) \begin{cases} \text{Minimize} & J\left[\mathbf{x}\left(\cdot\right), \mathbf{u}\left(\cdot\right), t_f\right] \\ \text{Subject to} & \dot{r} = v_r \\ & \dot{\theta} = v_t / r \\ & \dot{v}_r = v_t^2/r - 1/r^2 + f\sin\beta \\ & \dot{v}_t = -v_r v_t / r + f\cos\beta \\ & \mathbf{e}_L \leq \mathbf{e}_0\left(\mathbf{x}_0\right) \leq \mathbf{e}_U \\ & \mathbf{e}_f\left(\mathbf{x}_f\right) = \mathbf{0} \\ & t_0 = 0 \\ & t_f \leq t^U \end{cases} \tag{9}$$

The initial orbit is described by the endpoint function

$$\mathbf{e}_0\left(\mathbf{x}_0\right) := \begin{pmatrix} r - 1 \\ \left(v_t - 1\right)^2 + v_r^2 \\ v_t \\ v_r \end{pmatrix}, \qquad \mathbf{e}_L := \begin{pmatrix} 0 \\ 0 \\ 1 - \nu_{\max} \\ -\nu_{\max} \end{pmatrix}, \qquad \mathbf{e}_U := \begin{pmatrix} 0 \\ \nu_{\max}^2 \\ 1 + \nu_{\max} \\ \nu_{\max} \end{pmatrix}, \tag{10}$$

which we have modified to include the possibility of a lunar assist with a delta-v whose magnitude normalized by the Earth's orbital speed is defined as ν, with $\nu \in [0, \nu_{\max}]$.

The semi-major axis, a_f, and eccentricity, e_f, of the target orbit determine the second endpoint function

$$\mathbf{e}_f\left(\mathbf{x}_f\right) := \begin{pmatrix} a_f\left[\left(v_r^2 + v_t^2\right) r - 2\right] + r \\ r\left(1 + e_f\cos\theta\right) - \left(v_t r\right)^2 \\ v_r\left(1 + e_f\cos\theta\right) - e_f v_t \sin\theta \end{pmatrix}. \tag{11}$$

The maneuver time, t_f, is bound by t^U, for which we seek values that satisfy $t^U - t_f = \mathcal{O}(t_f) > 0$ for efficient convergence of the solution.

We note that the variables in Eqs. (7)-(11) are normalized such that lengths are in units of astronomical units (1 AU $= 1.49 \times 10^{11}$ m), velocities are in units of Earth's orbital speed (2.98×10^4 m/s) , accelerations are in units of Earth's centripetal acceleration (5.93×10^{-3} m/s^2), and time scales are in units of Earth's *angular* period ($1/2\pi$ years $= 5.02 \times 10^6$ s).

3. Lunar Assist

Case studies have shown that lunar assists on the outbound and inbound phases of the journey drastically increase the capability of ACR missions.[5,18] Therefore, we found it crucial to include the propellant mass savings of the lunar assist when developing our ACR mission model.

The maximum delta-v of a lunar assist is limited to about $\Delta v \approx 1.7$ km/s.[35] Consistent with the lunar assist used in the KISS study, we assume that the maximum excess hyperbolic velocity that can be either imparted to the outbound craft or removed from the inbound craft is about 1.4 km/s.[5] Therefore, we use the normalized value $\nu_{\max} = 0.047$ within Eq. (10).

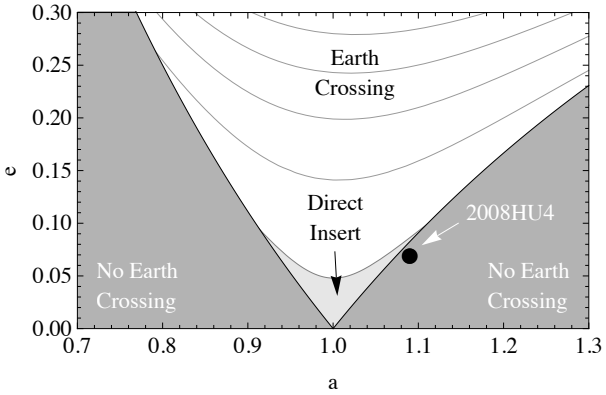

Figure 2. Phase space depiction of asteroid orbits within the ecliptic plane. a is the semi-major axis and e is the eccentricity. The solid grey region denotes orbits that do not cross the Earth's orbit. Grey lines correspond to surfaces of constant excess energy of the asteroid at the point of intersection with the Earth's orbit. The light gray region contains orbits whose energy is less than a critical value, where the critical value is defined as the energy that a lunar assist is capable of imparting to (for rendezvous with) or removing from (for capture of) the spacecraft. Also shown is the orbit of asteroid 2008HU4.

It is possible under the model presented in Sec. 2 to have a zero-cost transfer for certain target orbits. We illustrate this in Fig. 2 using a contour plot based on the analysis of Sanchez and McInnes.[10] In this plot, the grey contours represent lines of constant characteristic energy, or C_3. The dark grey region represents orbits that do not cross Earth, while the white region represents Earth-crossing orbits whose characteristic energy exceeds the maximum possible energy change provided by a lunar assist. The light grey region, however, contains Earth-crossing orbits that the spacecraft may be either directly inserted into of captured from using a lunar assist with magnitude $\nu \in [0, \nu_{\max}]$.

Also shown in Fig. 2 is the orbit of asteroid 2008HU4, which was the focus of the KISS case study. It is clear that this asteroid is right on the edge of the direct capture region. This is consistent with the criteria used in the study in which the target asteroid had both a close approach and a low approach speed.

Target orbits within the direct insert/capture region of Fig. 2 will be omitted from the remainder of our analysis. A detailed study of missions to these asteroids will need to include the relative phase between the departure orbit and destination orbit. Therefore, the departure date and close approach distance become important variables, thus rendering this problem beyond the scope of our model.

4. Time-Free Minimum-Fuel Transfers

In support of Eq. (6), we derive in this section a semi-empirical equation for the delta-v of the TFMF problem, Δv_ζ, by analyzing the solution to the optimal control equations outlined in Sec. 2 for 350 different target orbits and accelerations within the mission parameter space given by: $a_f \in [1.02, 1.40]$, $e_f \in [0, 0.25]$, and

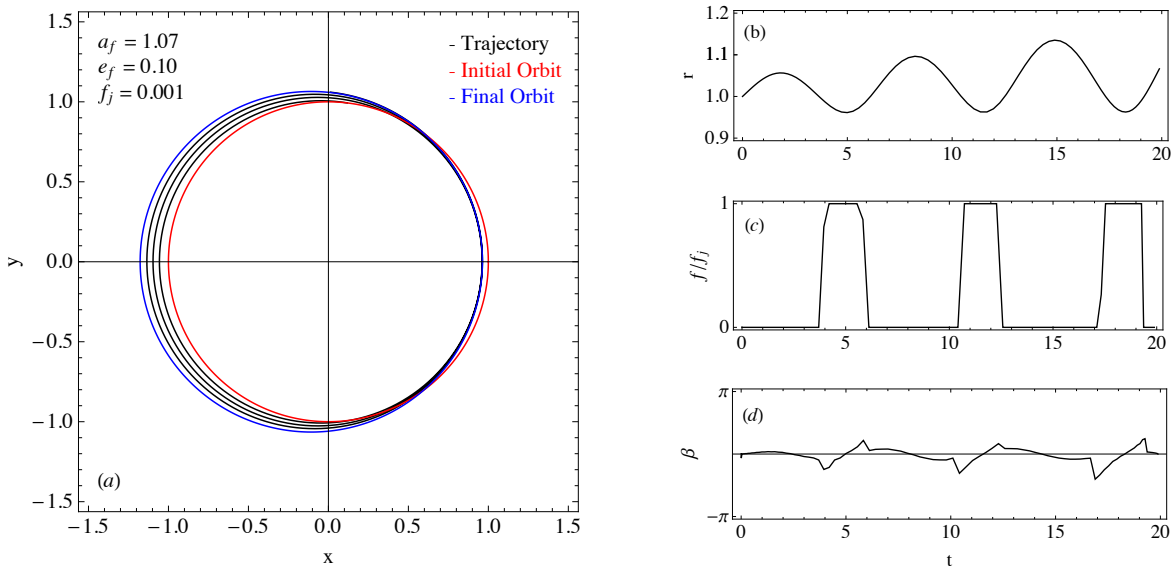

Figure 3. Example time-free minimum-fuel solution showing: (a) the trajectory in the ecliptic plane, (b) the radial distance from the sun, (c) the optimal acceleration control law, and (d) the optimal acceleration direction control law. The target orbit is characterized by $a_f = 1.07$ and $e_f = 0.10$, while the maximum acceleration is given by $f_j = 0.001$.

$f_j \in [0.005, 0.05]$. The cost function for a minimum-fuel transfer is given by $J_\zeta\left[\mathbf{x}\left(\cdot\right), \mathbf{u}\left(\cdot\right), t_f\right] = \int_{t_0}^{t_f} f dt$.[33] The equations are solved using the MATLAB-based software package DIDO,[36] and the control laws are verified by integrating the dynamical equations with a fourth-order Runge-Kutta solver.[37]

An example TFMF trajectory is shown in Fig. 3. The trajectory within the ecliptic plane, Fig. 3(a), reproduces the characteristic low-thrust spiral-orbit with approximately three revolutions for the given input parameters. Fig. 3(b) shows the normalized radial distance of the spacecraft from the sun. Peaks and valleys in Fig. 3(b) correspond the the apsides and periapsides of the spiral-orbit, respectively. It is evident from Fig. 3(c) that the optimal TFMF control law utilizes thrusting arcs while the spacecraft is near periapsis. Finally, Fig. 3(d) shows that the acceleration vector is applied mainly in the tangential direction.

The delta-v provided by the lunar assist may be written in vector form as $\Delta\mathbf{v} = \nu\cos\gamma\mathbf{e}_\theta + \nu\sin\gamma\mathbf{e}_r$, where $\mathbf{e}_\theta$ and $\mathbf{e}_r$ are the tangential and radial unit vectors, respectively. The optimal control problem in Sec. 2 is formulated such that the strength, ν, and angle, γ, of the lunar assist are free parameters of the optimization scheme. Therefore, the solution yields the optimal set of (ν, γ) for a given maneuver.

A strong correlation was observed between the strength of the lunar assist and the apsis of the target orbit, $r_a = a_f\left(1 + e_f\right)$ [Fig. 4(a)]. It is clear from this figure that ν scales linearly with r_a until a certain point after which the full capability of the lunar assist is required, or $\nu = \nu_{\max}$. The linear region can be understood as follows: if possible, the lunar assist should place the spacecraft into an orbit whose apsis is halfway between of the apsides of the target orbit and the initial orbit. Using this reasoning, the lunar assist magnitude may be formulated as

$$\nu = \begin{cases} 1 - \bar{r}_a^{-1/2} & \bar{r}_a < \bar{r}_a^* \\ \nu_{\max} & \bar{r}_a > \bar{r}_a^* \end{cases} . \tag{12}$$

Here, $\bar{r}_a \equiv 0.5(1 + r_a)$ is the average of the initial and final orbit apsides, and $\bar{r}_a^* \equiv (1 - \nu_{\max})^{-2}$. Fig. 4(a) indicates good agreement between the simple model and TFMF solution, with $\sim 90\%$ of the data points falling within $\sim 10\%$ of the model. Finally, Fig. 4(b) shows that $\gamma \ll 1$ over most of the parameter space, which indicates that the optimal lunar assist is most often applied along Earth's velocity vector.

Finding a correlation between $\Delta v_\zeta = J_\zeta$ and the mission parameters proved to be somewhat complex. For a given eccentricity, J_ζ was observed to be relatively constant as a_f increased. This proved true until the value $a_f = \left(1 - e_f\right)^{-1}$, after which J_ζ scaled according to $J_\zeta + \nu \approx 1 - a_f^{-1/2}$. We note that the

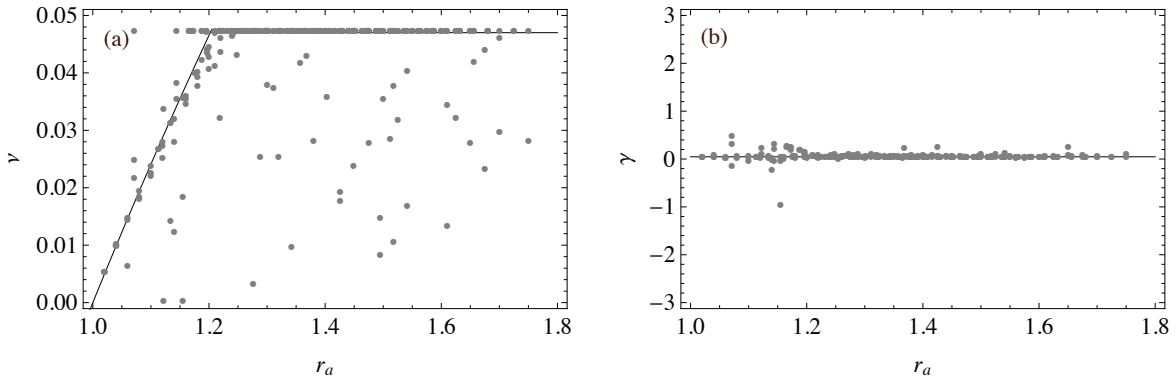

Figure 4. Scaling of the (a) optimal, normalized lunar assist delta-v magnitude, ν, and (b) direction, β, as a function of the apsis of the target orbit, r_a. The data points correspond to the numerical solution of the time-free minimum-fuel optimal control problem. The solid lines are obtained from Eq. (12).

quantity $1 - a_f^{-1/2}$ is the absolute velocity change of the spacecraft for a zero eccentricity final orbit. These observations led to the following model for Δv_ζ,

$$\Delta v_\zeta^* = \xi H(\xi), \tag{13}$$

where we define the quantities

$$\Delta v_\zeta^* \equiv \Delta v_\zeta + \sqrt{1 - e_f} + \nu - 1, \tag{14}$$

and

$$\xi \equiv a_f^{-1/2} \left(r_p^{1/2} - 1 \right). \tag{15}$$

In Eq. (13), H is the Heaviside step function and marks the transition between the two regions of different scaling. Interestingly, $\xi < 0$ corresponds to the Apollo class asteroids, whose orbits cross the Earth's orbit, and $\xi > 0$ the Amor asteroids, whose orbits do not cross the Earth's orbit. The agreement between the TFMF numerical solutions and the model of Eqs. (13-15) may be seen in Fig. 5(a).

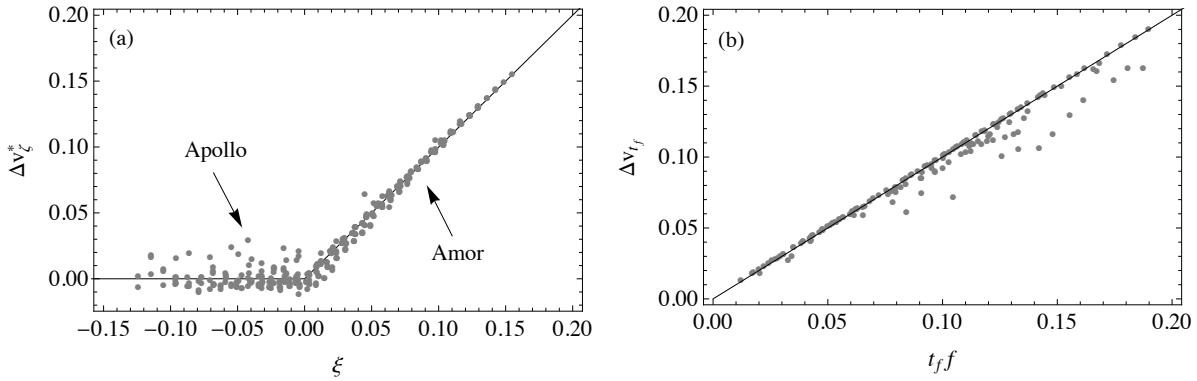

Figure 5. (a) Scaling of the time-free minimum-fuel delta-v, Δv_ζ, with the parameter ξ. The data points correspond to the numerically solution of the time-free minimum-fuel optimal control problem. The solid lines are obtained from Eqs. (13)-(15). Apollo and Amor asteroids correspond to $\xi < 0$ and $\xi > 0$, respectively. (b) Scaling of the minimum-time minimum-fuel delta-v, Δv_{t_f}, with the product of the maneuver time and acceleration, $t_f f$. The solid line corresponds to the "full throttle" control law.

5. Minimum-Time Minimum-Fuel Transfers

We apply the optimal control model of Sec. 2 to the MTMF problem over the same parameter space to determine an estimate for the remaining free parameter in Eq. (6), τ. Recall that $\tau \equiv t_{\min}/t_{\min}^* = f t_{\min}/\Delta v_\zeta$. The relevant cost function for the MTMF problem is $J_{t_f}\left[\mathbf{x}(\cdot), \mathbf{u}(\cdot), t_f\right] = t_f$.

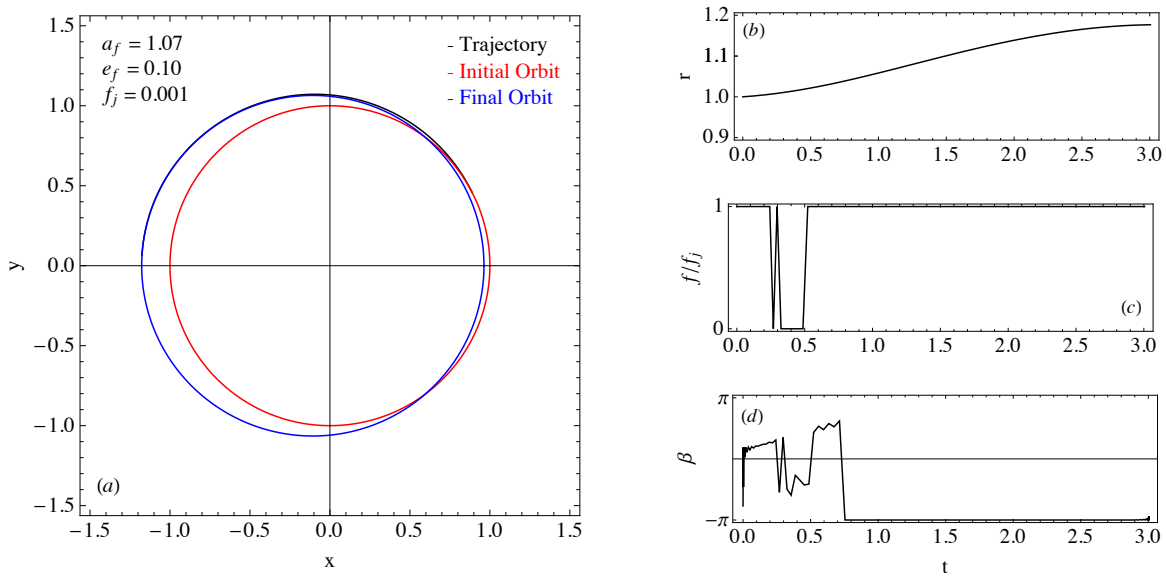

Figure 6. Example minimum-time minimum-fuel solution showing: (a) the trajectory in the ecliptic plane, (b) the radial distance from the sun, (c) the optimal acceleration control law, and (d) the optimal acceleration direction control law. The target orbit is characterized by $a_f = 1.07$ and $e_f = 0.10$, while the maximum acceleration is given by $f_j = 0.001$..

An example MTMF trajectory is shown in Fig. 6. Contrary to Fig. 3(a), Fig. 6(a) shows a very quick transfer from the initial orbit to the final orbit occurring near the orbital intersection. Fig. 3(b) shows that the normalized radial distance of the spacecraft from the sun monotonically increases for this transfer, thus indicating that the orbit does not go through a complete revolution. Fig. 3(c) demonstrates that the optimal MTMF control law utilizes near-continuous thrusting at maximum acceleration. However, Fig. 3(d) shows that the acceleration vector reverses direction nearly one-third the way through the maneuver, which suggests that the spacecraft is "braking" until it reaches the target orbit.

In Sec. 1 we made the assumption that the MTMF delta-v, Δv_{t_f}, is related to the maneuver time, t_f, by the "full-throttle" control law, or $\Delta v_{t_f} = t_f f$. We verify this assumption in Fig. 5(b), which shows that the vast majority of MTMF solutions fall within $\sim 20\%$ of the "full-throttle"-line for all of the MTMF solutions within our parameter space.

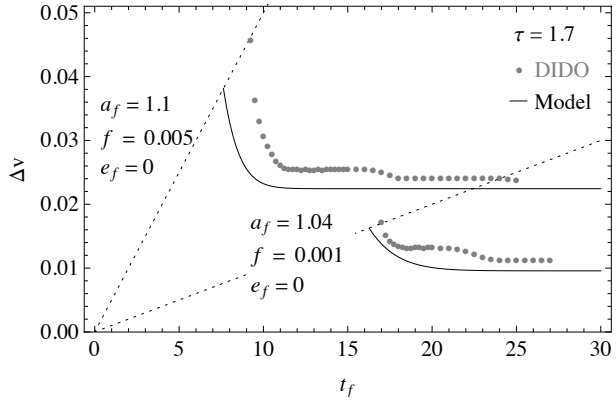

Figure 7. Delta-v, Δv, versus maneuver time, t_f, for the solution to the time-bound minimum-fuel optimal control problem (data points) and using the scaling model of Eq. (6) with $\tau = 1.7$. Solutions are presented for two different target orbits and accelerations. Dashed lines correspond to the "full throttle" control law.

Unfortunately, a clear correlation between τ and the mission parameters did not reveal itself over the chosen parameter space. We did, however, observe a slight decrease of τ with increasing a_f. Furthermore,

τ was seen to be independent of f_j for $f_j \leq 0.05$. As a result, we are forced to keep τ as a free parameter, with the additional insight that the MTMF solutions yield an approximate value of $\tau = 1.7 \pm 0.6$, which will be used throughout our analysis. A comparison between the model given by Eq. (6) with $\tau = 1.7$ and the numerical solution to the TBMF problem over a wide range of maneuver times for two different sets of mission parameters is shown in Fig. 7. We note that the under-prediction of Δv by Eq. (6) in the non-optimal region of the curve is consistent with the optimistic nature of our model.

IV. Maximum Return Mass Scaling

We are now in the position to return to the question posed at the outset: *How does the optimal electric propulsion system scale with the asteroid orbit and mass?* The mission time and mass balance, Eqs. (1) and (2), are related to the propulsion system and asteroid parameters through the Earth escape time and propellant mass fraction equations for phase one, Eqs. (3) and (4), and optimal rendezvous and return propellant mass fractions for phases two and three, Eq. (6).

We re-cast the power supply and propulsion system mass fraction in the more insightful form:

$$\rho = \frac{u_e f_2 \left(1 - \zeta_1\right)}{2\eta\alpha}. \tag{16}$$

Here, η is the thrust efficiency of the propulsion system and α is the power supply specific power. The model inputs are now the set of values corresponding to (t_2, t_3, f_2, u_e, η, α, δ, a_f, e_f). The accelerations of the other two mission phases, f_1 and f_3, result from f_2 and the overall mission mass balance.

We further constrain the problem by imposing the requirement that $t_2 + t_3 = t_{\text{syn}}$, where t_{syn} is the normalized synodic period of the target orbit, and is a function of only a_f. The time between close approaches between the asteroid and Earth scales approximately with the synodic period.[38] Therefore, this constraint implies that the departure and capture lunar assists occur at a time of close approach, which is consistent with the assumptions of our trajectory optimization model.

Furthermore, the time constraint implies $t_2 f_2 = t_3 f_3$, from which Eq. (6) yields $\zeta_2 = \zeta_3$. The inputs to the model are then reduced to (f_2, u_e, η, α, δ, a_f, e_f). The model is now sufficiently constrained to find the optimum acceleration, $\hat{f}_2$, and exhaust velocity, $\hat{u}_e$, as a function of the target orbit parameters, a_f and e_f, and the spacecraft and propulsion system performance specifications, δ, η, and α. Here, we define the optimum acceleration and exhaust velocity as the values that maximize the mass amplification ratio, μ.

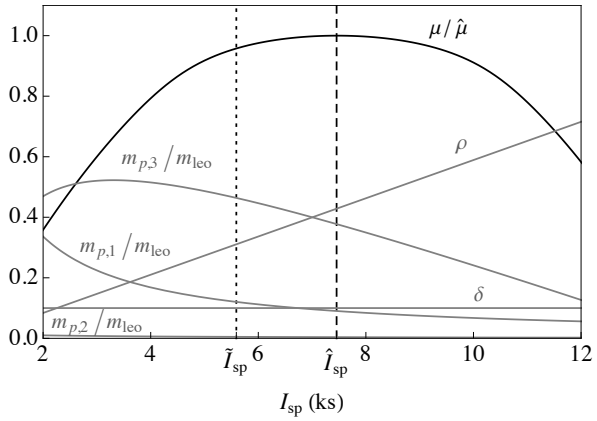

Figure 8. Spacecraft mass balance (gray lines) and mass amplification ratio (black line) for the target orbit $(a_f, e_f) = (1.07, 0.10)$ with $\alpha = 20$ W/kg, $\eta = 0.6$, and $\delta = 0.1$. $\hat{f}_2 = 1.54 \times 10^{-4}$ m/s^2 corresponds to the optimal value for the given orbit and specifications. The maximum mass amplification ratio is $\hat{\mu} = 86$ at $\hat{I}_{\text{sp}} = 7,456$ s. Near-optimal conditions are found to be $\tilde{I}_{\text{sp}} = 5,592$ s with $\tilde{\mu} = 82$.

A plot of the I_{sp}-dependance of μ and the various mass ratios for the target orbit $(a_f, e_f) = (1.07, 0.10)$ is shown in Fig. 8. In this example we take $\alpha = 20$ W/kg, $\eta = 0.6$, and $\delta = 0.1$. Furthermore, $\hat{f}_2 = 1.54 \times 10^{-4}$ m/s^2, which corresponds to the optimal value for the given orbit and specifications. Note that $m_{p,j}$ represents

the propellant mass consumed in the j^{th} mission phase. The maximum mass amplification ratio is defined as $\hat{\mu}$, which occurs at $I_{\rm sp} = \hat{I}_{\rm sp}$. Near $\hat{I}_{\rm sp}$, the majority of the mass inserted into LEO, $m_{\rm leo}$, consists of the power supply and propulsion system and the propellant used in the third phase of the mission. The propellant used in the first phase of the mission and the spacecraft mass also make up a non-negligible part of $m_{\rm leo}$. The propellant used in the second phase, however, is typically an order of magnitude lower than any of the other masses over the relevant specific impulse range.

The curves in Fig. 8 were found numerically using the implicit solution to Eq. (2) after substituting the delta-v model of Sec. II into the respective propellant mass fractions. It is possible using this method to find $\hat{u}_e$ and $\hat{f}_2$, and thus the optimal specific impulse and thrust (or power), for any target asteroid. While analyzing these solutions over a wide parameter space, we noticed a very simple and general trend emerge between the optimal power supply and propulsion system mass fraction and the spacecraft mass fraction, specifically $\hat{\rho} \approx 0.48\,(1-\delta)$. While the numerical method is useful in its generality, we use this insight to seek a less exact, yet more intuitive approximation for optimal propulsion system parameters.

We begin by defining a modified mass amplification ratio

$$\mu^* \equiv \frac{u_e\,(1-\delta-\rho)}{\Delta v_\zeta}, \tag{17}$$

where μ^* takes into account the spacecraft, power supply and propulsion system, and third phase propellant mass balance in the limit $\Delta v_3 \to \Delta v_\zeta$. We will eventually add a correction for the non-negligible first phase propellant mass (e.g. see Fig. 8).

With the goal of finding an analytical solution for the optimal power supply and propulsion system mass fraction, $\hat{\rho}$, we use Eq. (16) to rewrite u_e in terms of ρ and f_2,

$$u_e = u_e^* + \Delta v_1, \tag{18}$$

where we have defined

$$u_e^* \equiv \frac{2\eta\alpha\rho}{f_2}. \tag{19}$$

We substitute Eqs. (18) and (19) into Eq. (23) and solve for the extremum. This ultimately produces the following analytical equation for $\hat{\rho}$ in terms of $\hat{f}_2$ and the mission parameters:

$$\hat{\rho} = \frac{1}{2}\,(1-\delta) - \frac{\hat{f}_2 \Delta v_1}{4\eta\alpha}. \tag{20}$$

Indeed, we were able to show that the numerical solutions over a wide parameter space collapsed entirely onto the line described by Eq. (20). Furthermore, substitution of Eq. (19) into Eq. (20) yields

$$\hat{\rho} \approx \frac{1}{2}\left(1 - \frac{\Delta v_1}{2\hat{u}_e^*}\right)(1-\delta)\,, \tag{21}$$

in the limit where $\Delta v_1 / u_e^* \ll 1$. The first term in brackets is typically ~ 0.95, thus we have recovered the general trend that emerged from the numerical solutions. The meaning of Eq. (21) is the following: to maximize the return mass of the asteroid, the mass of the propulsion system and power supply should be nearly equal to the mass of propellant used throughout the entire mission.

Eq. (20) is significant because, if a similar scaling relation for $\hat{f}_2$ can be found, Eqs. (18) and (19) give a closed-form analytical equation for $\hat{u}_e$. Indeed, using the numerical solution to the mass optimization problem over a wide parameter space and least-squares fitting the data, we found that $\hat{f}_2$ approximately follows the scaling relation,

$$\hat{f}_2 \approx 10^{-4} t_{\rm syn}^{-0.5}\,(\tau/1.7)^{0.5}\,(\alpha\eta)^{0.53}\left(6\delta^2 + 0.04\right)^{-0.12}. \tag{22}$$

Here, $\hat{f}_2$ is given in m/s^2, $t_{\rm syn}$ is given in years, α is given in W/kg, and all other variables are dimensionless. We note that Eq. (22) was observed to reproduce the numerical solution to within a few percent.

We add the propellant mass of the first phase to the modified mass amplification ratio to arrive at an approximate equation for the maximum mass amplification,

$$\hat{\mu} = \hat{\mu}^* - \frac{\Delta v_1}{\Delta v_\zeta}, \tag{23}$$

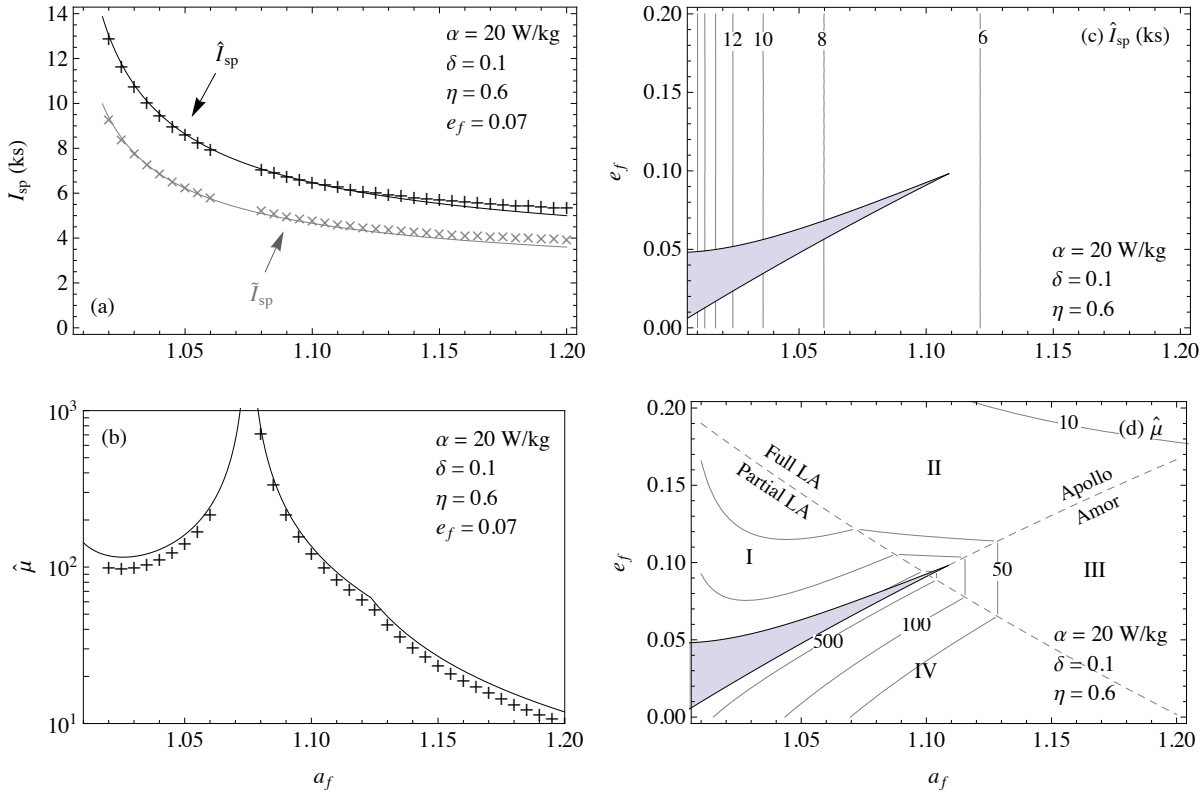

Figure 9. Scaling of the maximum return mass solutions. A comparison is shown between the numerical solution (crosses) to Eq. (2) and the semi-empirical model (lines) of Eqs. (23-22) for (a) the optimal and near-optimal specific impulses, $\hat{I}_{sp}$ and $\tilde{I}_{sp}$, respectively, and (b) maximum mass amplification, $\hat{\mu}$. Orbital phase space (a_f-e_f) contour plots are presented for (c) $\hat{I}_{sp}$, (d) $\hat{\mu}$. Dashed lines represent the division between Apollo and Amor asteroids, and orbits that do and do not utilize a full lunar assist. The shaded region corresponds to direct insertion orbits of Fig. 2.

where $\hat{\mu}^*$ is evaluated using Eqs. (18-20) and (22).

Finally, we note that the curve for μ vs. I_{sp} is not strongly peaked near $\hat{I}_{sp}$, which is exemplified in Fig. 8. Therefore, a small sacrifice in the return mass may be used to obtain a significant decrease in the required specific impulse. We define the *near-optimal* specific impulse, $\tilde{I}_{sp}$, as the specific impulse required to bring back 95% of the maximum possible mass, or $\tilde{\mu} = 0.95\hat{\mu}$. Substituting this metric into Eq. (23) with $\tilde{f}_2 = \hat{f}_2$, it can be shown that the near optimal conditions are well-approximated by: $\tilde{I}_{sp} \approx 0.75\hat{I}_{sp}$, $\tilde{\rho} \approx 0.75\hat{\rho}$.

The value of the optimal specific impulse from Eq. (18) and near-optimal specific impulse as a function of the semi-major axis of the target orbit, a_f, for $\alpha = 20$ W/kg, $\eta = 0.6$, $\delta = 0.1$, and $e_f = 0.07$ are shown in Fig. 9(a). Also shown are data points corresponding to the numerical solution to Eq. (2) for optimality and near-optimality. It is evident that the optimum specific impulse of the longer duration missions (lower a_f) is much higher than the shorter duration missions (higher a_f). This is because longer duration missions may be completed with much lower levels of thrust, and therefore higher specific impulses.

Scaling of the maximum mass amplification ratio may be seen in Fig. 9(b). The asymptote in these figures corresponds to the direct-insertion region described in Sec. 3. For the Amor asteroids, with $a_f(1 - e_f) > 1$, this implies that $\hat{\mu}$ increases drastically as the close approach distance decreases. The increase observed as the Apollo asteroid orbits approach the asymptote can be explained by a decreased relative velocity between the Earth and asteroid at the point of their orbital intersection. These results extend the findings of Landau *et. al*,[18] who concluded that the return mass of the asteroid can be maximized at a fixed-I_{sp} by decreasing the close approach distance and relative velocity.

Contour plots of the optimal specific impulse and mass amplification ratio as a function of the target asteroid orbit may be seen in Figs. 9(c)-(d) for $\alpha = 20$ W/kg, $\eta = 0.6$, and $\delta = 0.1$. The shaded regions of these plots correspond to the direct insertion region of Fig. 2. It is clear that $\hat{I}_{sp}$ is independent of e_f, which

results from the time constraint on the second and third mission phases.

The dashed lines in Fig. 9(d) represent to the division of the Apollo and Amor asteroids, and target orbits whose optimal trajectories use either a partial or full lunar assist [see Eq. (12)]. Fig. 9(d) indicates that the scaling of $\hat{\mu}$ varies over four distinct regions in the following manner:

I. Apollo + Partial LA: The maximum return mass is large near the direct-insertion region, but falls off rapidly as the relative velocity between the asteroid and Earth at the orbital intersection increases. The increase in the returnable mass as $a_f \to 1$ is a result of the rapidly increasing mission time.

II. Apollo + Full LA: The maximum return mass is somewhat independent of a_f, and rapidly decreases for increasing e_f.

III. Amor +Partial LA: The maximum return mass is mostly independent of e_f, and rapidly decreases for increasing a_f.

IV. Amor + Full LA: The maximum return mass scales mainly with the periapsis of the target orbit, and rapidly increases as the distance between the periapsis approaches Earth's semi-major axis. The maximum values in this region are higher than those in region I.

Thus, the results of our mission model imply that the most desirable targets are Amor asteroids whose periapsis approaches Earth's semi-major axis ($r_p \to 1$) and whose apsis satisfies $r_a < 2\left(1-\nu_{\max}\right)^{-2} - 1$, where $\nu_{\max}$ is the maximum delta-v of the lunar assist normalized by Earth's orbital speed. Apollo asteroids whose semi-major axis approaches that of Earth's also provide large return mass opportunities, however their large synodic period implies unreasonable mission durations. Finally, both Apollo and Amor asteroids whose orbits require a full lunar assist are attractive targets near the full lunar assist boundary, but rapidly become unattractive away for that boundary. We note that an increase of around $\sqrt{2}$ in the returnable mass for asteroids in this region is observed by extending the mission duration to $2t_{\text{syn}}$, however, this value is still much lower than the best region III asteroids.

We complete this section with a discussion of the values obtained for the optimal and near-optimal specific impulse and mass amplification ratio. As we mentioned in Sec. 5, the shape of the non-optimal region of the Δv-t_f curve within our model depends on the free parameter, τ. By solving for $\hat{I}_{\text{sp}}$, and $\hat{\mu}$ while varying τ, we find that the uncertainty in the values presented in Fig. 9 are around 20% for τ within the limits observed by the MTMF solutions. More accurate values may be obtained if a scaling relation for τ can be found in terms of the parameters of the model, however, we note that a 20% uncertainty is likely consistent with the uncertainties inherent to the assumptions of our simplified model.

V. Conclusions

We presented a simple model for the mission time and mass constraints of an asteroid capture and return mission based on the propellant requirements of each mission phase. Using numerical results from the nonlinear optimization software, DIDO, we derived scaling laws for the propellant requirements of the rendezvous and return phases of the mission based on the maneuver time and the asteroid orbit and propulsion system parameters. Constraining the rendezvous and return phases of the mission by the synodic period of the target asteroid, we used the mass conservation equation to numerically solve for the optimum specific impulse, and developed from this solution a semi-empirical equation for the optimal and near-optimal specific impulse, and mass amplification ratio.

Emerging from this model was a simple scaling relation between the optimal power supply and propulsion system mass ratio and the spacecraft mass ratio. From this relation we can define a power coefficient,

$$C_P \equiv \frac{P}{\alpha m_{\text{leo}}\left(1-\delta\right)}, \tag{24}$$

which relates the power, P, to the specific power, α, spacecraft mass ratio, δ, and total spacecraft mass in low-Earth orbit, m_{leo}. Eq. (21) implies that the maximum mass amplification of an ACR mission requires $C_P \approx 1/2$, while a mission capable of 95% of the maximum mass amplification requires $C_P \approx 3/8$. This simple result is general and accurate to $\mathcal{O}\left(\Delta v_1 / 2u_e^*\right)$. We note that the power increases with the specific power of the power supply due to the increased return mass capability. In other words, for a given asteroid mass, m_{leo} decreases as α increases.

It was determined by the KISS case study that "sufficiently powerful" electric propulsion systems are an enabling technology for asteroid capture and return missions.[5] Their results showed that an 18.8 ton spacecraft equipped with *near-term* power and propulsion technology (four 10 kW/3,000 s Hall thrusters operating on 40 kW solar power) is capable of returning a 1,300 ton asteroid. The results from our model, on the other hand, can be used to determine the *far-term* requirements of electric propulsion systems needed to maximize the capability of asteroid capture and return missions. The deliverable mass to LEO of current (and former) launchers is on the order of $10^4 - 10^5$ kg. For a specific power of 20 W/kg, our model implies that propulsion systems capable of processing 100 kW – 1 MW of power with a specific impulse in the range 5,000 – 10,000 s have the potential to return asteroids on the order of $10^3 - 10^4$ tons.

Acknowledgements

The first author would like to thank Dr. I. M. Ross and Elissar Global for offering student discounts on DIDO, technical support, and for making the program incredibly intuitive. He would also like to thank Mykola Bordyuh for finding the original Tsiolkovsky quote and source.

References

[1]Tsiolkovsky, K. E., Исследование Мировых Лространств Реактивными Лриборами, 1910-1911.

[2]Barucci, M., Dotto, E., and Levasseur-Regourd, A. C., "Space missions to small bodies: asteroids and cometary nuclei," The Astronomy and Astrophysics Review, Vol. 19, No. 1, 2011, pp. 1–29.

[3]Gao, Y., Li, H.-N., and He, S.-M., "First-round design of the flight scenario for Change-2s extended mission: takeoff from lunar orbit," Acta Mechanica Sinica, Vol. 28, No. 5, 2012, pp. 1466–1478.

[4]Jutzi, M., Asphaug, E., Gillet, P., Barrat, J.-A., and Benz, W., "The structure of the asteroid 4 [thinsp] Vesta as revealed by models of planet-scale collisions," Nature, Vol. 494, No. 7436, 2013, pp. 207–210.

[5]Brophy, J., Friedman, L., Culick, F., et al., "Asteroid Retrieval Feasibility Study," Tech. Rep. N/A, Keck Institute for Space Studies, Califonia Institute of Technology, Jet Propulsion Laboratory, April 2, 2012.

[6]Hills, J. G., "Capturing asteroids into bound orbits around the earth: Massive early return on an asteroid terminal defense system," Tech. Rep. LA-UR–92-466, Los Alamos National Lab., NM (United States), 1992.

[7]Massonnet, D. and Meyssignac, B., "A captured asteroid: Our David's stone for shielding earth and providing the cheapest extraterrestrial material," Acta Astronautica, Vol. 59, No. 1, 2006, pp. 77–83.

[8]O'Leary, B., "Mining the Apollo and Amor asteroids," Science, Vol. 197, No. 4301, 1977, pp. 363–366.

[9]Lewis, J. S., Mining the sky: untold riches from the asteroids, comets, and planets, Addison-Wesley Pub. Co., Reading, MA, 1996.

[10]Sanchez, J. and McInnes, C., "Asteroid resource map for near-Earth space," Journal of Spacecraft and Rockets, Vol. 48, No. 1, 2011, pp. 153–165.

[11]Elvis, M., "Let's mine asteroids—for science and profit," Nature, Vol. 485, 2012, pp. 549.

[12]Shoemaker, E. and Helin, E., "Earth-approaching asteroids as targets for exploration," NASA Conference Publication, Vol. 2053, 1978, pp. 245–248.

[13]Barucci, M. A., Cheng, A., Michel, P., et al., "MarcoPolo-R near earth asteroid sample return mission," Experimental Astronomy, Vol. 33, No. 2-3, 2012, pp. 645–684.

[14]Garca Yrnoz, D., Sanchez, J., and McInnes, C., "Easily retrievable objects among the NEO population," Celestial Mechanics and Dynamical Astronomy, 2013, pp. 1–22.

[15]Brophy, J. R., Gershman, R., Strange, N., Landau, D., Merrill, R., and Kerslake, T., "300-kW Solar Electric Propulsion System Configuration for Human Exploration of Near-Earth Asteroids," 47th AIAA/ASME/ASEE Joint Propulsion Conference and Exhibit, No. AIAA-2011-5514, July 31-August 3, 2011.

[16]Landau, D. and Strange, N., "Near-Earth asteroids accessible to human exploration with high-power electric propulsion," AAS/AIAA Astrodynamics Specialist Conference, Vol. 11, 2011.

[17]Brophy, J. R., Gershman, R., Landau, D., Yeomans, D., Polk, J., Porter, C., Williams, W., Allen, C., and Asphaug, E., "Asteroid return mission feasibility study," 47th AIAA/ASME/ASEE Joint Propulsion Conference and Exhibit, No. AIAA-2011-5665, July 31-August 3, 2011.

[18]Landau, D., Dankanich, J., Strange, N., Bellerose, J., Llanos, P., and Tantardini, M., "TRAJECTORIES TO NAB A NEA (NEAR-EARTH ASTEROID)," Tech. Rep. AAS 13-409, NASA/Caltech-JPL and NASA/GRC, 2013.

[19]Hasnain, Z., Lamb, C. A., and Ross, S. D., "Capturing near-Earth asteroids around Earth," Acta Astronautica, Vol. 81, No. 2, 2012, pp. 523–531.

[20]Jahn, R. G., Physics of Electric Propulsion., McGraw-Hill Book Co., Div. of McGraw-Hill, Inc., New York, NY.

[21]Choueiri, E. Y., Kelly, A. J., and Jahn, R. G., "Mass savings domain of plasma propulsion for LEO to GEO transfer," Journal of Spacecraft and Rockets, Vol. 30, No. 6, 1993, pp. 749–754.

[22]Shoemaker, E. M., Williams, J., Helin, E., and Wolfe, R., "Earth-crossing asteroids: Orbital classes, collision rates with Earth, and origin," Asteroids, Vol. 1, 1979, pp. 253–282.

[23]Bottke Jr, W. F., Morbidelli, A., Jedicke, R., Petit, J.-M., Levison, H. F., Michel, P., and Metcalfe, T. S., "Debiased orbital and absolute magnitude distribution of the near-Earth objects," Icarus, Vol. 156, No. 2, 2002, pp. 399–433.

[24]Gronchi, G. F. and Valsecchi, G. B., "On the possible values of the orbit distance between a near-Earth asteroid and the Earth," Monthly Notices of the Royal Astronomical Society, Vol. 429, No. 3, 2013, pp. 2687–2699.

[25]Wiesel, W. E., Spaceflight dynamics, Vol. 2, Mcgraw-hill New York, 1989.

[26]Edelbaum, T. N., "Optimum low-thrust rendezvous and station keeping," AIAA Journal, Vol. 2, No. 7, 1964, pp. 1196–1201.

[27]Lee, S., von Ailmen, P., Fink, W., Petropoulos, A., and Terrile, R. J., "Design and optimization of low-thrust orbit transfers," Aerospace Conference, 2005 IEEE, IEEE, 2005, pp. 855–869.

[28]Abdelkhalik, O. and Taheri, E., "Approximate On-Off Low-Thrust Space Trajectories Using Fourier Series," Journal of Spacecraft and Rockets, Vol. 49, No. 5, 2012, pp. 962–965.

[29]Oh, D. Y. and Landau, D., "Simple Semi-Analytic Model for Optimized Interplanetary Low-Thrust Trajectories Using Solar Electric Propulsion," Journal of Spacecraft and Rockets, 2013, pp. 1–11.

[30]McConaghy, T. T., Debban, T. J., Petropoulos, A. E., and Longuski, J. M., "Design and optimization of low-thrust trajectories with gravity assists," Journal of spacecraft and rockets, Vol. 40, No. 3, 2003, pp. 380–387.

[31]Sivardiere, J., "Symmetry and the derivation of invariant vectors for planar motions," American Journal of Physics, Vol. 62, 1994, pp. 328–328.

[32]Gobetz, F. W., "Optimal variable-thrust transfer of a power-limited rocket between neighboring circular orbits," AIAA Journal, Vol. 2, No. 2, 1964, pp. 339–343.

[33]Ross, I. M., "Space trajectory optimization and L1-optimal control problems," Modern Astrodynamics, Vol. 1, 2006, pp. 155–188.

[34]Ross, I. M., Gong, Q., and Sekhavat, P., "Low-thrust, high-accuracy trajectory optimization," Journal of Guidance, Control, and Dynamics, Vol. 30, No. 4, 2007, pp. 921–933.

[35]Niehoff, J. C., "Gravity-assisted trajectories to solar-system targets." Journal of Spacecraft and Rockets, Vol. 3, No. 9, 1966, pp. 1351–1356.

[36]Ross, I. M., "A Beginners Guide to DIDO (Ver. 7.3)," A MATLAB Application Package for Solving Optimal Control Problems, Elissar, LLC, 2007.

[37]Butcher, J. C., Numerical methods for ordinary differential equations, John Wiley & Sons, 2008.

[38]Baalke, R. and Yeomans, D., "Near Earth Object Program," Jet Propulsion Laboratory (http://neo.jpl.nasa.gov/).